Received: 15 April 2021 | Revised: 10 March 2022 | Accepted: 22 March 2022

DOI: 10.1002/jbm.b.35066

RESEARCH ARTICLE

Society For Biomaterials | WILEY

Comparison of modern light-curing hybrid resin-based composites to the tooth structure: Static and dynamic mechanical parameters

Nicoleta Ilie

Department of Conservative Dentistry and Periodontology, University Hospital, LMU Munich, Munich, Germany

Correspondence
Nicoleta Ilie, Department of Conservative Dentistry and Periodontology, University Hospital, LMU Munich, Goethestr. 70, D-80336 Munich, Germany
Email: nilie@dent.med.uni-muenchen.de

Abstract

The study aims to compare the way modern resin-based composites (RBCs) respond to mechanical stress related to the tooth structure they are designed to replace. Eight representative light-cured RBCs, including ormocers, giomers, RBCs with nano and agglomerated nanoparticles, prepolymerized, or compact fillers, were selected. Flexural strength, FS and modulus/E, were measured in a three-point bending test. A fractographic analysis determined the origin of fracture. The quasi-static (indentation hardness/H_{IT}, indentation modulus/E_{IT}) and viscoelastic (storage modulus/E', loss modulus/E'', loss factor/tan δ) behavior was assessed by a depth-sensing indentation test equipped with a dynamic-mechanical analysis module. One and multiple-way analysis of variance (ANOVA), Tukey honestly significant difference (HSD) post-hoc tests ($\alpha = 0.05$), and Weibull statistics were applied. Parameter *material* exhibited the highest effect on E ($p < .001$, $\eta_P^2 = .857$), followed by FS ($\eta_P^2 = .729$), and the strain ($\eta_P^2 = .553$). Highest material reliability was identified in the RBCs with nano and agglomerated nanoparticles. The most frequent type of failure originated from volume (81.3%), followed by edge (10.6%), and corner (8.1%) flaws. Enamel evidenced three times higher H_{IT}, E_{IT}, and E' values as RBCs and dentin, and the smallest deviation from ideal elasticity. Ormocers exhibited the highest damping capacity, followed by the RBCs with prepolymerized fillers. Damping capacity and static mechanical properties are mutually exclusive. Analyzed RBCs and the tooth structure are better adapted to the relevant frequency for chewing than for higher frequencies. RBCs are comparable to dentin in terms of their mechanical performance, but apart from the damping behavior, they are far inferior to enamel. Damping ability of analyzed material could be exploited for correlation with the clinical behavior.

KEYWORDS
dynamic-mechanical analysis, resin-based composites, tooth structure, viscoelasticity

1 | INTRODUCTION

Resin-based composites (RBCs) were developed with the purpose to efficiently replace the damaged tooth structure. Similar to the tooth structure, RBCs consist of organic and inorganic components, which are connected to one another, evidencing local inhomogeneity and graded properties.[1,2] The presence of collagen in the natural tooth structure or of polymer in RBCs in addition to the friction occurring at the interphase boundary or inherent defects lead to pronounced viscoelastic behavior[3] in both the natural tooth structure[4,5] and in the RBCs.[6] The response of viscoelastic materials to external load is one intermediate between an elastic solid and a viscous liquid, involving a time-dependent recovery.[3] This behavior cannot be assessed by conventional static tests as they mainly focus on the elastic behavior of the material and are less appropriate for relating the physical properties to the structure of the material.[7] A well-suited method to describe the viscoelastic material behavior is the dynamic-mechanical analysis (DMA).[7] When DMA is performed through nano-indentation techniques, it enables both the clinical conditions and the small dimensions of the samples to be taken into account. The method involves the use of oscillatory (sinusoidal) components at frequencies that can mimic chewing activity in humans, that occur at 0.94 to 2.17 Hz,[8] in addition to higher frequencies, that enable to detect structural differences in the substrates.[7] The measured delay between strain and force oscillations (phase shift, δ) in such tests permit dividing the complex modulus in an elastic portion (storage modulus, E'), which reveals the ability of the material to store elastic energy associated with recoverable elastic deformation, and a viscous portion (loss modulus, E''), which characterizes the dissipated energy.[7] In addition, the ratio of the viscous to the elastic material response defines a parameter with high clinical relevance, the loss factor (tan δ), which is not yet sufficiently exploited for the interpretation of the clinical behavior of dental materials. It is a measure of the damping behavior of the material and reflects its energy dissipation potential. Recent studies have clearly shown that dental glass ceramics have a consistently lower ability to absorb shock (smaller tan δ) compared to industrially cured computer-aided design (CAD)/computer-aided manufacturing (CAM) RBCs.[6] This requires an in-depth analysis of the clinical susceptibility of these materials to chipping or fracturing associated with tan δ.

The clinical success of a restoration with direct, light-cured RBCs is indisputably a multifactorial event. In this context, the mechanical properties of the materials are ascribed an important role.[9,10] This statement relates both to the correlation of the clinical performance of RBC restorations with mechanical properties such as flexural strength[11] and to the reason for the failure of the RBC restorations in a clinical situation.[9] An extensive analysis of the clinical studies published in the periods 1995–2005 and 2006–2016[9] reveal significant changes in the clinical behavior of RBC restorations depending on the decade of observation. The survival rates of posterior RBC restorations in these two decades are given as 89.41% and 86.87%, which shows hardly any difference. However, the causes of failure have changed remarkably. In the period 1995–2005, the main reasons for failure were secondary caries (29.47%) and RBC fractures (28.84%), while tooth fractures (3.45%) were rarely observed. In comparison, RBC fracture (39.07%) was found to be the main reason for posterior restoration failure in 2006–2016, followed by secondary caries (25.68%) and tooth fracture (23.76%).[9] The result of this comparison clearly evidence an increase in the incidence of RBC and tooth fractures in recent years. On a positive note, the same study attested a decrease in secondary caries, postoperative sensitivity, and RBC wear.[9] Clinically, this shift in the cause of failure can be explained on the one hand by the use of RBCs in increasingly larger restorations, but on the other hand it also reflects changes in RBCs properties over the decades,[10] since improved aesthetic is usually achieved by reducing the filler size with the consequence of decreasing mechanical properties.[10]

Modern light-cured RBCs offer a great variation in the chemical composition of the individual components, their distribution, interaction and morphology, which enable fine-tuning towards improved bioactivity[12] and mechanical performance,[13] lower shrinkage,[14] and improved polishability and aesthetic.[15] Among them, hybrid RBCs are the most common restorative materials used clinically.[15] Their subdivision into nano-, micro-, and submicrometer hybrid RBCs is more of a commercial nature and is nondiscriminatory in view of the mechanical properties.[13] Within the hybrid RBCs, the greatest differences are related to the type, structure, and properties of the reinforcing filler. Crystalline (e.g., zirconia, silica) versus amorphous (glasses), chemically inert versus bioactive, compact versus complex three-dimensionally structured (nano- and nanoclusters), smooth versus porous surfaces, single versus multicomponent (e.g., prepolymerized) fillers are used either individually or as a complex mixture within a single material.[15] Bioactive fillers such as surface prereacted glass (S-PRG) fillers are used less frequently as chemically inert fillers, but they proved successful as they were able to ensure stable mechanical properties[16] in addition to a remineralization effect.[12] The S-PRG fillers are made from a fluoroaluminosilicate glass which, in the presence of water, forms a silicate hydrogel with a polyalkenoic acid. The hydrogel is then freeze-dried, ground, and silanised.[17,18] In addition to fluorides, the release of other ions such as Na^+, Sr^{2+}, Al^{3+}, BO_3^{3-}, SiO_3^{2-} was also detected.[12] These fillers are incorporated into an organic matrix to form bioactive RBCs that are branded as giomers.[17]

Even if the focus of the improvements in RBCs was on the modification of the filler system, the composition of the organic matrix was not neglected. It contains dimethacrylates such as bisphenol A glycol dimethacrylate (Bis-GMA), ethoxylated bisphenol A dimethacrylate (Bis-EMA), urethane dimethacrylate (UDMA), triethylene glycol dimethacrylate (TEGDMA), but also complex derivatives of these monomers. As such, Ormocers (organically modified ceramic) are based on UDMA modifications[19] that were developed with the aim of reducing shrinkage by using large matrix monomers with few cross-links.[14] They consist of inorganic Si–O–Si networks based on

polysiloxanes, which were produced using a sol–gel process and were crosslinked by polyfunctional urethane and thioether (meth) acrylate.[20]

The aim of this study was therefore to quantify the static and viscoelastic properties of representative, modern light-cured hybrid RBCs in relation to the tooth structure (enamel and dentin). Based on the trends described above and without the objective being exhaustive, a number of 8 hybrid RBCs was selected. The selection includes Ormocers, Giomers, RBCs with nano and agglomerated nanoparticles, RBCs with prepolymerized, and with compact fillers. Furthermore, this comparison should be carried out in a large-frequency range, from 1 to 50 Hz, thus including the chewing relevant frequencies (0.94 to 2.17 Hz[8]).

The tested null hypotheses were that analyzed RBCs will behave similarly with regard to a) strength, elastic modulus, strain, Weibull parameters, and fracture pattern; b) viscoelastic (storage modulus E', loss modulus E'', loss tangent tan δ) and quasistatic mechanical properties (indentation hardness H_{IT}, indentation modulus, E_{IT}) as well as their variation pattern with the frequency (1 to 50 Hz); and c) the viscoelastic and quasistatic mechanical properties of the RBCs is similar to the tooth structure.

2 | MATERIALS AND METHODS

The flexural strength, FS, and flexural modulus, E, were determined in a three-point bending test. The fractured specimens were then all analyzed fractographically. The quasistatic and viscoelastic behavior of the analyzed RBCs and the tooth structure was monitored by an instrumented indentation test equipped with a DMA module (FISCHERSCOPE® HM2000, Helmut Fischer, Sindelfingen, Germany). Eight light-cured, hybrid RBCs were selected and are described as Ormocers (AF, AFO), Giomers (BLS), RBCs with nano and agglomerated nanoparticles (FSE, FSB, FSD), RBCs with prepolymerized (BEG, BLS) and RBCs with compact filler (GSO) (Table 1). The examined materials were tested in a common shade for dental restoratives (A3). The light-emitting diode (LED) light curing unit (LCU) Bluephase® Style (Ivoclar Vivadent, Schaan, Liechtenstein) with an irradiance of 1412 mW/cm^2, which was measured by a spectrophotometer (MARC, Managing Accurate Resin Curing) System; Bluelight Analytics Inc., Halifax, Canada) was used for polymerization.

2.1 | Three-point bending test

The flexural strength, FS, and flexural modulus, E, were determined in a three-point bending test according to NIST No. 4877 with a distance of 12 mm between the supports,[21] and ISO 4049:2009.[22] For this purpose, 160 ($n = 20$) specimens were produced by compressing the material between two glass plates with polyacetate sheets in between, which were separated by a polyoxymethylene mold with an inner dimension of 2 mm × 2 mm × 18 mm. The specimens were overlapped polymerized from top and bottom as specified in ISO 4049:2009[22] for 20 s (AFO for 40 s, as specified by the manufacturer) and stored in artificial saliva (pH 6.9; 1000 mL: 1.2 g potassium chloride, 0.84 g sodium chloride, 0.26 g dipotassium phosphate, 0.14 g calcium chloride dehydrate) at 37 °C immediately after demolding for 24 h. Specimens were loaded until fracture in a universal testing machine (Z 2.5, Zwick/Roell, Ulm, Germany) at a crosshead speed of 0.5 mm/min. The universal testing machine measured the force during bending as a function of the deflection of the beam. The flexural modulus was calculated from the slope of the linear part of the force–deflection diagram. The deflection at fracture (D) was also recorded and used to calculate the strain (ε) in mm/mm, or multiplied by 100%, the strain (ε) in percentage.

$$\varepsilon = \frac{\Delta l}{l_0} = \frac{6\,D d}{{l_0}^2}$$

where D = maximum deflection of the center of the beam, (mm); d = thickness of tested beam, (mm); and l_0 = support span, (12 mm).

2.2 | Fractography analysis

The fractography was performed with a stereomicroscope (Stemi 508, Carl Zeiss AG, Oberkochen, Germany) in order to determine the fracture pattern. All fractured surfaces were photographed using a microscope extension camera (Axiocam 305 color, Carl Zeiss AG, Oberkochen, Germany). The origin of fracture was identified either as volume (sub-surface) or surface (edge, corner) defects. Three specimens for each fracture mode were then selected and sputtered with a gold–palladium coating for scanning electron microscopy (Zeiss Supra 55VP, Carl Zeiss GmbH, Göttingen, Germany).

2.3 | Instrumented indentation test (IIT)

2.3.1 | Quasistatic indentation test

Fragments ($n = 6$) resulted from the three-point bending test were wet-ground with silicon carbide abrasive paper (grit size p1200, p2500, and p4000, LECO Corporation) and polished with a diamond suspension (mean grain size: 1 μm) for 2–3 min, until the surface was shiny (automatic grinding machine EXAKT 400CS Micro Grinding System EXAKT Technologies Inc. OK). Tooth specimens of 2 mm thickness were obtained from six caries-free human molars (ethics committee approval for using anonymized extracted teeth, No. 21-0426KB). For this purpose, one slice per tooth was cut perpendicular to the long axis of the tooth, and was polished similar to the RBC specimens.

The ratio of the elastic reverse deformation work of indentation (W_{elast}) and the total mechanical work of indentation (W_{total}) was

TABLE 1 Analyzed RBCs: Abbreviation (code), brand, manufacturer, shade, LOT and composition, as indicated by the manufacturer

						Filler	
Code	Material	Manufacturer	Shade	LOT	Monomer	Composition	wt/vol%
BEG	Brilliant EverGlow	Coltene	A3	I60409	TEGDMA, Bis-GMA	PPF, SiO_2, BaO-Al_2O_3-SiO_2	79/64 (total) 74/56 (inorganic)
BLS	Beautifil II LS	Shofu	A3	051814	UDMA, Bis-MPEPP; Bis-GMA, TEGDMA	PPF, S-PRG B_2O_3-F-Al_2O_3-SiO_2	83/69
GSO	Grandio SO	VOCO	A3	1832173	Bis-GMA, Bis-EMA TEGDMA	Glass–ceramic SiO_2	89/73
FSE	Filtek Supreme XTE Enamel	3 M ESPE	A3	N941498	Bis-GMA, Bis-EMA, UDMA, TEGDMA, PEGDMA	SiO_2, ZrO_2	78.5/63.3
FSB	Filtek Supreme XTE Body	3 M ESPE	A3	N961392	Bis-GMA, Bis-EMA, UDMA, TEGDMA, PEGDMA	SiO_2, ZrO_2	78.5/63.3
FSD	Filtek Supreme XTE Dentin	3 M ESPE	A3	N963106	Bis-GMA, Bis-EMA, UDMA, TEGDMA, PEGDMA	SiO_2, ZrO_2	78.5/63.3
AF	Admira Fusion	VOCO	A3	1830088	Ormocer	SiO_2	84/ n.s.
AFO	Admira Fusion	VOCO	OA3	1830478	Ormocer	SiO_2	84/ n.s.

Abbreviations: B_2O_3-F-Al_2O_3-SiO_2 = boroaluminosilicate glass; BaO-Al_2O_3-SiO_2, barium aluminosilicate glass; Bis-EMA, ethoxylated bisphenol A dimethacrylate; Bis-GMA, bisphenol A glycol dimethacrylate; Bis-MPEPP, bisphenol A polyethoxy methacrylate; n.s., not specified; Ormocer, organically modified ceramic; PEGDMA, poly(glycerol 1,3-dimethacrylate); PPF, Pre-polymerized filler; SiO_2, silicon oxide (silica); S-PRG = surface pre-reacted glass ionomer filler; TEGDMA, triethylene glycol dimethacrylate; UDMA, urethane dimethacrylate; ZrO_2, zirconium oxide.

assessed ($W_{elast}/W_{total} = \mu_{IT}$) according to ISO 14577[23] by using an automated nano-indenter (FISCHERSCOPE® HM2000) equipped with an Vickers diamond tip. This parameter is a prerequisite for the DMA test. For this purpose, one measurement per specimen was carried randomly ($n = 6$) for each specimen, RBC brand, enamel, and dentin. The indentation was performed force controlled and at room temperature; the test load increased within 20 s, was kept constant for 5 s and then decreased within 20 s with constant speed in the range 0.4 to 1000 mN. Load (F) and indentation depth (h) of the indenter were continuously measured during the load–unload cycle, allowing calculating the elastic and plastic deformation. A part of the mechanical work W_{total} ($= \int F dh$) during the indentation procedure is consumed as plastic deformation work W_{plast}, while the rest is set free as work of the elastic reverse deformation $W_{elastic}$.

During indentation an impression is produced with a projected area of contact of the indenter (A_c) determined from the force/indentation depth curve, taking into account the indenter correction based on the Oliver and Pharr model and described in ISO 14577.[23] The indenter area function was therefore calibrated on two different materials with uniform and well-known material properties (sapphire and fused quartz). Corrections obtained from the tip calibration are then used for further computational data evaluation. The indentation hardness ($H_{IT} = F_{max}/A_c$) is a measure of the resistance to plastic deformation. This value is convertible to HV (Vickers hardness). The indentation modulus (E_{IT}) was calculated from the slope of the tangent of indentation depth-curve at maximum force.[23]

2.4 | Dynamic mechanical analysis

The DMA test used a low-magnitude oscillating force (20 different frequencies in the range 1–50 Hz) that was superimposed onto a quasistatic force of 1000 mN. The indenter was therefore driven towards the surface of the specimen under computer control. An initial static force of 1000 mN was applied within 30 s and held at that tip position, followed by applying the oscillating load to the tip. Then the static force was released within an additional 30 s. The oscillation amplitude was set at 5 nm, so that the sample deformation kept within the linear viscoelastic regime. Ten repeated measurements were performed per each frequency and indentation. Six randomly chosen indentations have been performed per each specimen, amounting 36 individual indentations per RBC brand, enamel, and dentin. For the used frequency (1.0; 1.2; 1.5; 1.9; 2.3; 2.8; 3.4; 4.2; 5.2; 6.4; 7.8; 9.6; 11.8; 14.5; 17.9; 21.9; 26.9; 31.1; 40.7; and 50.0 Hz), the force oscillation generates oscillations on the displacement signal with a phase angle δ. The sinusoidal response signal was then separated into a real part and an imaginary part representing the storage (E') and the loss moduli (E''), respectively. E' is a measure of the elastic response of a material behavior, whereas E'', characterizes the viscous material behavior. The quotient E''/E' is defined as the loss factor (tan δ) and is a measure of the material damping behavior.

The applied frequency (ω) and force (F_0) are preset parameters. The amplitude (X) and phase (ϕ) of the response are measured parameters. For each used frequency (ω), the force oscillation generates

oscillations on the displacement signal with a phase angle (ϕ). The displacement response is given as:

$$x = X\sin(\omega t - \varphi)$$

The contact for a dynamic test can be modeled by a single degree of freedom, damped, forced harmonic oscillator, while using the stiffness (k) and the damping (C), with m being the indenter mass:

$$F_0\sin(\omega t) = m\ddot{x} + C\dot{x} + kx$$

Solutions to these differential equations are:

$$X = \frac{F_0}{\sqrt{(k - m\omega^2)^2 + (C\omega)^2}} \text{ and } \varphi = \tan^{-1}\frac{\omega C}{k - m\omega^2}$$

Following, k and C can be expressed as:

$$k = \frac{F_0}{X}\frac{1}{\sqrt{1 + \tan^2\varphi}} + m\omega^2$$

and

$$C = \sqrt{\frac{\left(\frac{F_0}{X}\right)^2\tan^2\varphi}{1 + \tan^2\varphi}}\left(\frac{1}{\omega}\right)$$

In this equation k and C are the combined stiffness and damping of the sensor (s) and the sample (i).

$$k = k_i + k_s \text{ and } C = C_i + C_s$$

The stiffness and damping of the sensor were determined in the calibration of the sensor in air. The stiffness and damping of the sample can then be directly subtracted from the measured values. These calculated values for stiffness and damping of the sample are then used to determine the storage modulus (E'), loss modulus (E''), and tanδ (E'/E''). The equations which represent these are given below.[24]

$$E' = \frac{k_s\sqrt{\pi}}{2\sqrt{A_c}}\,E'' = \frac{\omega C_s\sqrt{\pi}}{2\sqrt{A_c}}\,\tan\delta = \frac{C_s\omega}{k_s}$$

2.5 | Statistical analyses

The distribution of the variables was tested with the Shapiro–Wilk procedure. All variables were normally distributed enabling using a parametric approach. Multifactor analysis of variance was applied to compare the parameters of interest (flexural strength FS, flexural modulus E, strain, fracture mode, storage modulus E', loss modulus E'', loss tangent tan δ, indentation hardness H_{IT}, and indentation modulus E_{IT}) among analyzed materials, tooth structure and loading frequencies. The results were compared using one- and multiple-way analysis of variance (ANOVA) and Tukey honestly significant difference (HSD) post hoc-test using an alpha risk set at 5%. A multivariate analysis (general linear model) assessed the effect of parameters *material* and *frequency* as well as their interaction terms on the analyzed properties. The partial eta-squared statistic reported the practical significance of each term, based on the ratio of the variation attributed to the effect. Larger values of partial eta-squared (η_P^2) indicate a greater amount of variation accounted for by the model (SPSS Inc. Version 25.0, Chicago, IL).

FS data have been additionally described by a Weibull analysis. A common empirical expression for the cumulative probability of failure P at applied stress σ is the Weibull model[25]:

$$P_f(\sigma_c) = 1 - \exp\left[-\left(\frac{\sigma_c}{\sigma_0}\right)^m\right]$$

where σ_c is the measured strength, m the Weibull modulus, and σ_0 the characteristic strength, defined as the uniform stress at which the probability of failure is 0.63. The double logarithm of this expression gives: $\ln\ln\frac{1}{1-P} = m\ln\sigma_c - m\ln\sigma_0$. By plotting ln ln(1/[1 − P]) versus lnσ_c, a straight line results, with the upward gradient m, whereas the intersection with the x-axes gives the logarithm of the characteristic strength.[25]

3 | RESULTS

The parameters measured in the three-point bending test are summarized in Table 2 and Figure 1. One-way ANOVA evidenced three homogeneous subgroups for FS data, which are related to each other in the following material sequence (AF, BLS, AFO, BEG; $p = .914$) < (GSO, FSE, FSD; $p = .18$) < (FSE, FSD, FSB; $p = .223$). Flexural modulus, E, data were graded more discriminative in five homogeneous subgroups: (AFO, AF, BLS; $p = .379$) < (BLS, BEG; $p = .749$) < (FSE, FSD; $p = .998$) < (FSD, FSB; $p = .142$) < GSO. A multifactorial analysis evidenced a significant influence of the parameter *material* ($p < .001$) while the effect was highest on the E ($\eta_P^2 = .857$), followed by the FS ($\eta_P^2 = .729$), and the strain ($\eta_P^2 = .553$). The highest material reliability was identified in the RBCs with nano and agglomerated nanoparticles (FSE, FSB, FSD), followed by the groups AF, BLS and GSO, BEG AFO (Table 2).

The fracture mode distribution (Figure 2) evidenced failures initiated from volume defects (subsurface mode) as the most frequent type of failure (81.3%), followed by failures initiated by edge (10.6%) and corner (8.1%) defects. A representative example of each of these three fracture mechanisms is shown in Figure 3.

The parameter μ_{IT} varied between 25.1% (dentin) and 52.6% (FSE). The total indentation work (W_{total}) was lowest in enamel (1.3 μJ) and increased significantly in the sequence GSO (2.3 μJ) < (FSB, FSD, FSE, $p = .433$; 2.6 μJ −2.7 μJ) < (AF, AFO, dentin, BEG, $p = .528$; 3.08–3.17 μJ) < BLS (3.5 μJ). Lowest elastic indentation work (W_{el})

TABLE 2 Three-point bending test

	FS, MPa		Weibull parameters			E, GPa		ε, %	
RBC	Mean	SD	m	σ_0	R^2	Mean	SD	Mean	SD
AF	125.4^{a}	12.6	11.7 (0.4)	130.9	0.98	5.4^{a}	0.4	2.6^{bc}	0.3
BLS	126.2^{a}	12.6	11.4 (0.6)	131.9	0.95	5.8^{ab}	0.6	2.4^{b}	0.2
AFO	129.9^{a}	18.5	7.0 (0.7)	139.1	0.86	5.3^{a}	0.5	2.8^{c}	0.5
BEG	131.3^{a}	18.2	8.5 (0.3)	138.9	0.98	6.1^{b}	0.4	2.4^{b}	0.4
GSO	163.5^{b}	21.6	9.0 (0.3)	172.6	0.98	10.8^{e}	0.8	1.6^{a}	0.2
FSE	173.7^{bc}	12.9	16.0 (0.9)	179.4	0.94	7.2^{c}	1.1	2.6^{bc}	0.3
FSD	175.6^{bc}	10.7	18.7 (2.2)	180.6	0.80	7.4^{cd}	0.6	2.6^{bc}	0.3
FSB	185.3^{c}	6.7	33.4 (2.0)	188.3	0.94	8.0^{d}	1.0	2.6^{bc}	0.2

Note: Data are arranged in ascending order of the flexural strength, FS. FS, the Weibull parameters (*m* with standard error in parenthesis; characteristic strength σ_0 which is the strength at a probability of failure *F* of 63.2%, and R Square [R^2] values), the flexural modulus *E* (mean and standard deviation, *SD*) and the strain ε are specified below; Superscript letters designate homogeneous groups within analyzed materials and measured property; Tukey's HSD (honestly significant difference) post-hoc test ($\alpha = .05$).

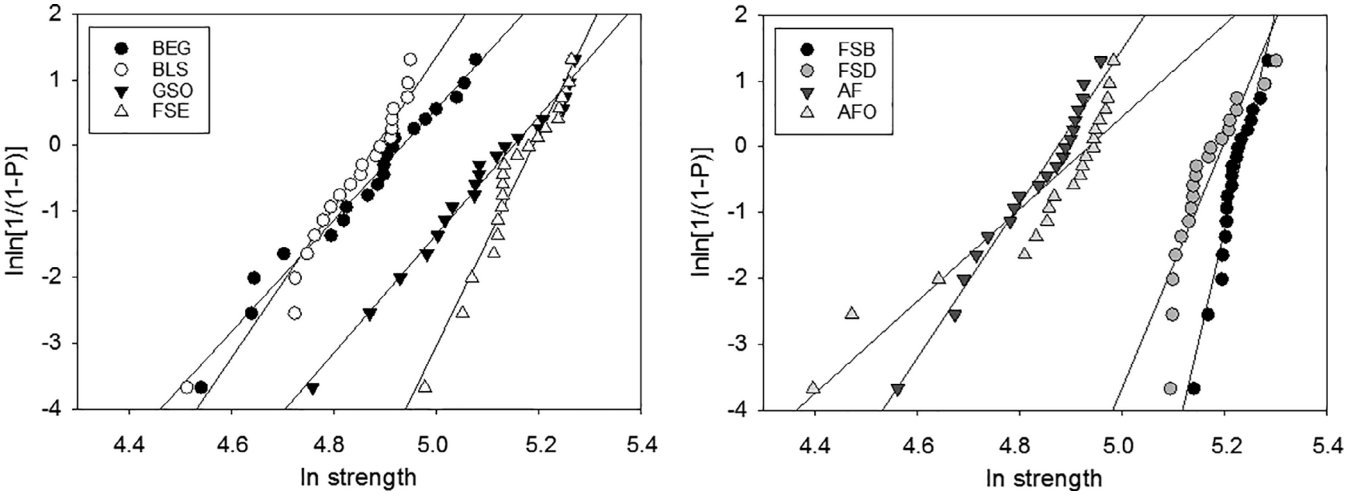

FIGURE 1 Weibull plot representing the empirical cumulative distribution function of strength data. Linear regression was used to numerically assess goodness of fit and estimate the parameters of the Weibull distribution, as summarized in Table 2

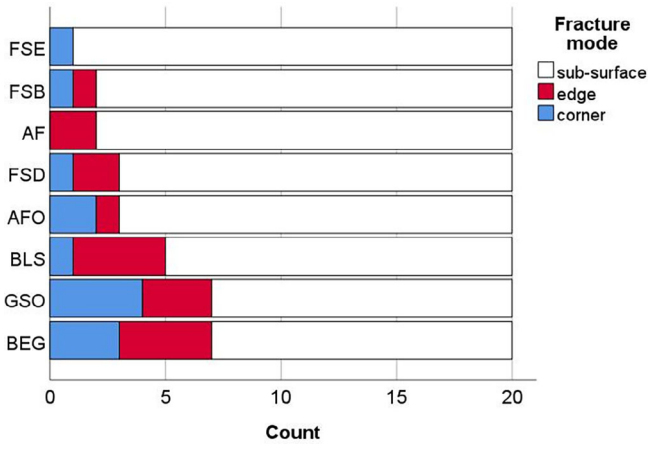

FIGURE 2 Fracture mode distribution among analyzed RBCs

was measured in enamel (.49 μJ) and increased significantly in the sequence: dentin (.78 μJ) < (FSB, FSD, $p = .765$; 1.31–1.36 μJ) < (FSD, FSE, $p = .383$; 1.36–1.43 μJ) < (FSE, AFO, BEG, $p = .579$; 1.43–1.48 μJ) < (AFO, BEG, BLS, AF, $p = .146$; 1.47–1.56 μJ).

The highest H_{IT}, E_{IT}, and storage modulus E' values at all frequencies were recorded for the enamel, followed by GSO at very large distance. The order of materials then differs in relation to the measured property, as illustrated in Figures 4B and 5B on an adapted scale. H_{IT} data differentiate the highest values in the statistical similar group of FSB, FSE, and FSD ($p = .892$), followed by AF, while the other analyzed materials, including dentin, are ranked lowest. In contrast to H_{IT} data, the dentin evidenced the highest E_{IT} and E' values and is then followed by a similar material sequence as described for H_{IT}. It should be noted that within a measured property all materials vary in a comparable pattern with

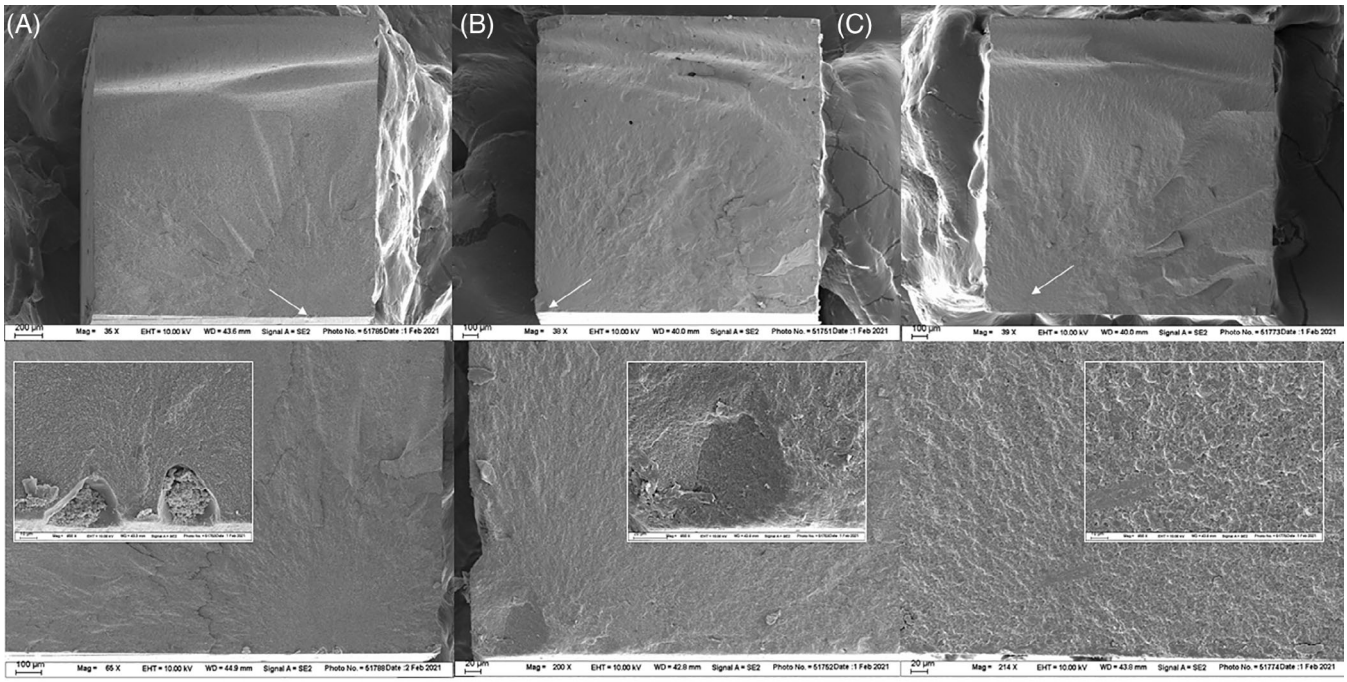

FIGURE 3 SEM-images: (A) fracture originated from an edge defect (BEG, FS = 133.9 MPa); (B) fracture originated from a defect at the corner (BLS FS = 125.5 MPa); (C) fracture originated from a sub-surface defect (FSB, FS = 189.6 MPa). Arrows indicate the defect located in the tensile zone. The defect and the fracture mirror are shown enlarged below

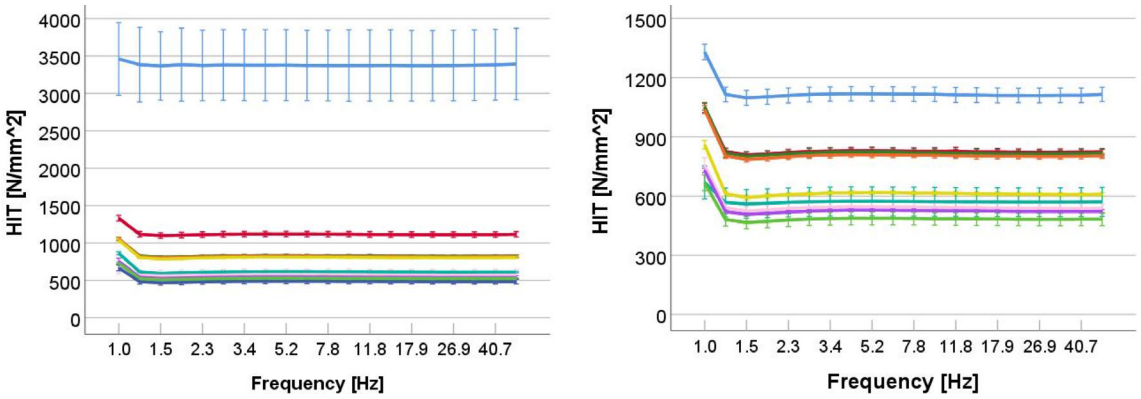

FIGURE 4 H_{IT} over the frequency range 1–50 Hz for the analyzed materials (left, A). A close-up without enamel is shown in the diagram on the right (B)

frequency. Differences in the variation pattern are registered within measured property, as the highest values are reached at the lowest frequency for H_{IT}, while the opposite is valid for E_{IT} and E'. In addition, H_{IT} curves plateau earlier (1.9 Hz) than the E_{IT} and E' curves (2.8 Hz), while parameters E_{IT} and E' differ less.

The variation of the loss modulus (E'') with the frequency showed that the enamel behaves differently again. It displayed a very high value at the lowest frequency, which then steadily decreases with frequency up to a plateau at very low values. GSO, FSB, FSE, FSD also show, in addition to dentin, a steady decrease in E'' with frequency, but started from a much lower value. This behavior stays in contrast to the variation of E'' identified in the other materials that evidenced a peak before the steady decrease. All curves then lead to a plateau at a frequency of 11.8 Hz (Figure 6).

The highest values for the loss factor (tan δ) were observed at the lowest frequency in all materials (Figure 7). The tan δ decreased toward zero at higher frequencies in enamel. Similar to E'' the decrease in tan δ with the frequency is steadily up to 11.8 Hz. GSO and dentin performed statistically similar ($p = .640$), as did FSB, FSE, and FSD ($p = .685$). Highest tan δ values were recorded in AF and AFO, which plateau at a high value, above 0.4.

A multifactorial analysis reveal a significant ($p < .001$) and high influence of the analyzed *substrate* (RBCs, dentin, and enamel) and *frequency* as well as their interaction product on the measured

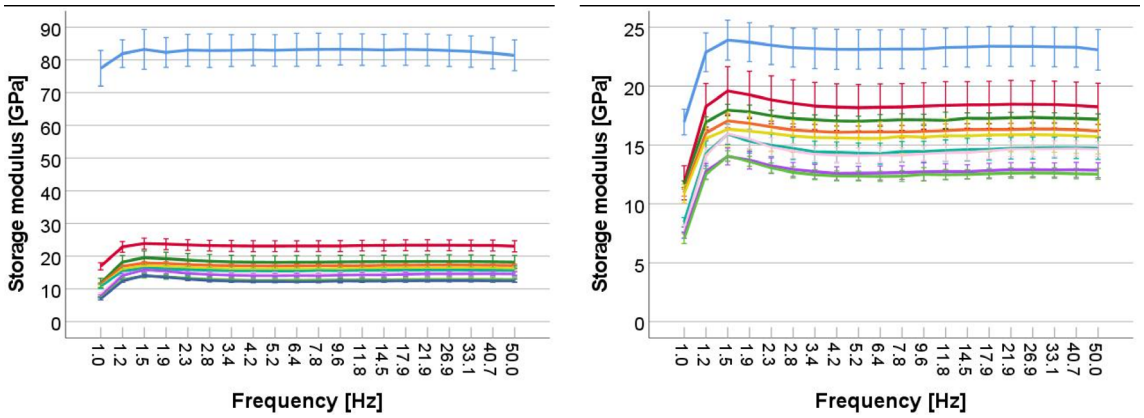

FIGURE 5 Storage modulus (E') over the frequency range 1–50 Hz for the analyzed materials (left, A). A close-up without enamel is shown in the diagram on the right (B)

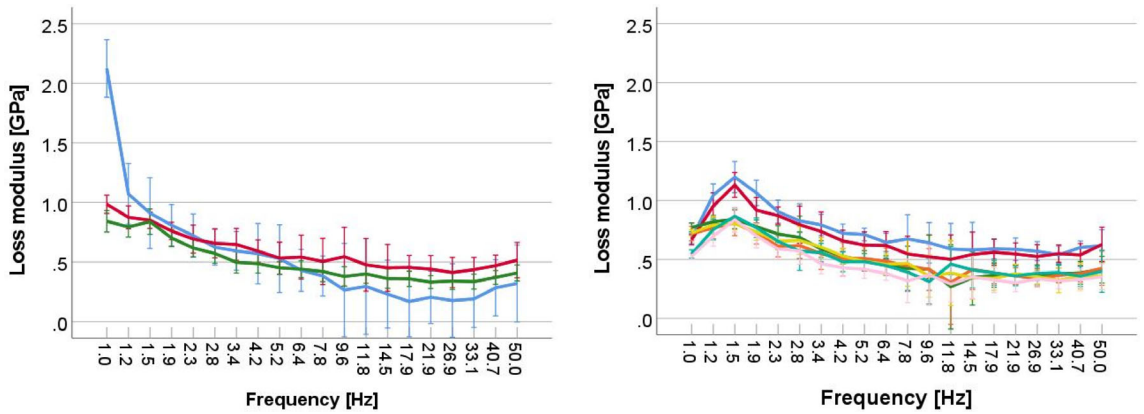

FIGURE 6 Loss modulus (E'') over the frequency range 1–50 Hz, highlighting three characteristic variation patterns

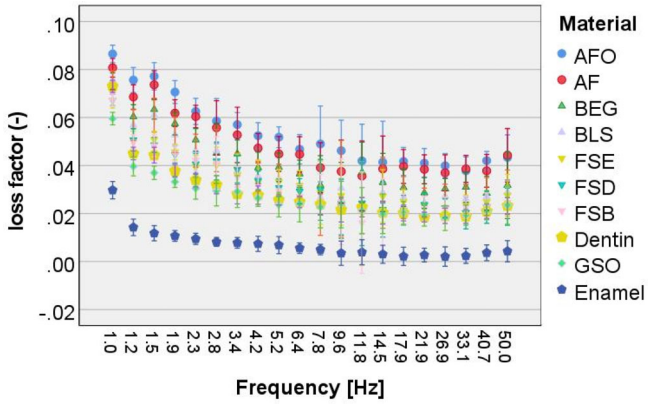

FIGURE 7 Loss factor over the frequency range 1–50 Hz

properties. The effect of the parameter *substrate* was highest on H_{IT} ($\eta_P^2 = .966$), followed by E_{IT} and E' ($\eta_P^2 = .92$ for both), tan δ ($\eta_P^2 = .77$), and was lowest on E'' ($\eta_P^2 = .223$). *Frequency* affected highest tan δ ($\eta_P^2 = .872$), followed by E'' ($p < .001$, $\eta_P^2 = .576$), E' and E_{IT} ($\eta_P^2 = .267$), and H_{IT} ($\eta_P^2 = .05$). The interaction product *substrate* × *frequency* exerted an effect only on E'' ($\eta_P^2 = .433$) and tan δ ($\eta_P^2 = .180$).

4 | DISCUSSION

RBCs improvement relates on the detailed analysis and understanding of the clinical behavior of previous materials and the correlation between chemical composition, microstructure and properties. The character of dental RBCs as complex composite materials between organic polymers and inorganic fillers rises high demands on this analysis, as parameters that have been determined so far in standardized laboratory tests rarely and only weakly correlate with the clinical behavior.[10] Parameters that show a certain correlation with the clinical behavior of the materials, such as flexural strength and hardness,[10,11] were among the parameters determined in the present study, while parameters such as the damping ability can, at least intuitively, be associated with clinical issues like chipping, and could be exploited for correlation with the clinical behavior in further studies. Based on the current state of knowledge, it is accepted that the prediction of the clinical behavior of a material requires the determination of a battery of parameters,[10] while the search for appropriate parameters is an ongoing process.

New restorative materials strives to mimic the structurally optimized mechanical functionality of the tooth structure in terms of

being hard and stiff as well as damage-tolerant. A direct comparison of the properties of the tooth structures and the RBCs is possible through the use of tests such as the IIT and the DMA. However, measurements with low indentation forces and depths are fraught with potential for error and misleading results, thus requiring a series of conditions to be fulfilled. In addition, one must be aware that although standards for elastic–plastic material behavior are available[23] and are incorporated into many commercial devices such as the one used in the present study, there is currently no standard for testing the mechanical behavior of viscoelastic materials, which holds a lot of potential for discussion in the choice of proper measurement conditions.

One of the first premises for correct results is the use of uncontaminated sample surfaces with a surface roughness that is lower than the penetration depth.[26] To ensure this, an automatic grinding machine was used to create accurate flat specimens, which were then polished to a high gloss and thoroughly cleaned, as described above. The lowest indentation depth in the present study exceed the surface roughness by far, as it varied from 4 to 5 μm, and occurred in enamel. The decision to work with indentation depths of several μm aimed to prevent another source of error, namely the indentation size effect (ISE) phenomenon. This effect became relevant at penetration depths below 1 μm[26] and is a scale-dependent material behavior that manifests as an increase or more seldom a decrease in hardness with decreasing indentation depth. It should also be taken into account that modeling the relationship between the contact depth and the indentation depth which is measured by the indentation technique, is still a point of debate,[27] since it is not trivial due to eventual pile-up or sink-in phenomenon that can occur during indentation. These effects cannot only be determined with tip displacement measurements and may lead to errors in the absolute measurement of mechanical properties. To account for these effects, several methods of indenter tip shape calibration have been developed, with the most popular based on Oliver and Pharr's analysis, which was implemented also in the standard used in the present study.[23,28] For DMA tests, the model used in the present study consists in determining the area below the loading–unloading curve, which permits the calculation of work performed during indentation, as described in Section 2. The projected contact area calculated with this method was estimated to be very close to the value calculated with the Oliver and Pharr model,[23,28] yet the model is less precisely for indentation on samples showing a pile-up phenomenon.[27] The latter is, however, a material response usually observed in metals.[29]

Further inaccuracies in material properties obtained through the instrumented indentation test when probing viscoelastic materials such as polymers are connected to the indenter geometry,[30] as pyramidal,[31] spherical,[32,33] or flat punch[34] probes have different applicability. Their choice should be determined by the desire to obtain dynamic stiffness and damping measurements that are dominated by the response of the sample.[30] Sharp indenters such as the Berkovich (three-sided pyramid) or Vickers (four-sided pyramid) are very popular and widely used in nano- and microinstrumented indentation experiments, but their application to characterize the mechanical properties of viscoelastic polymers is seen controversial in the literature and was either deemed appropriate[35] or has been questioned,[31] as a pyramid indenter failed to generate a contact consistent with the assumptions of linear viscoelasticity. In contrast, a flat punch indenter can ensure that the contact area remains constant during both the loading and unloading cycle even in the presence of creep behavior if the creep rate is not too high,[30] but it cannot guarantee perfect parallelism between the tip and the sample, so that there is always a small tilt angle that need to be taken into account. Stress concentration along the contact edge is another disadvantage of using such an indenter.[34] For probing efficiently the viscoelasticity of polymers a spherical tip is often recommended.[32,33] Since the investigated materials are based on polymers, but are heavily filled with inorganic particles, their viscoelasticity is low compared to a pure polymer matrix, so that they can be assumed to be elastic materials with regard to the contact area estimation. Using a Vickers indenter to probe viscoelastic properties for the analyzed materials can therefore be an acceptable compromise.

In the present study design, the tooth enamel showed a striking behavior compared to dentin or the analyzed RBCs. It evidenced three times higher H_{IT}, E_{IT}, and E' values as the highest values achieved in the RBCs and in the dentin, in addition to the smallest deviation from ideal elasticity, as quantified by the smaller tan δ and its decrease toward zero at higher frequencies. These results can directly be related to the chemical composition and the microstructure of the enamel, which is a highly mineralized material consisting of 96% by weight and 90% by volume of hydroxyapatite[36] and a protein matrix. The mineral amount in enamel is far higher than the inorganic filler amount in any of the materials analyzed (Table 1). Although the high mineral content is responsible for the hardness and modulus of elasticity of enamel, it is the arrangement and organization of its mineral and nonmineral components that modulate the way the enamel reacts to stress.[37] The smallest structural unit in enamel are apatite crystallites, which are grouped into more complex and larger-scale structures, the prisms. In turn, a prism is a closely packed parallel rod-like structure, evidencing a keyholes shape with diameters of ~5 μm.[37] There is no evidence of an interprismatic substance, but the orientation of the crystallites in the interprismatic regions seems to differ from those of the rod cores. These less densely packed transition regions allowed the accumulation of proteins and water and are described as distinct protein-rich structures.[37] For this study, measurements in enamel were carried out at random in six teeth without distinguishing the specifics of the microstructure at different locations. The depth of indentation in the enamel at a static indentation force of 1000 mN varied from 4 to 5 μm, while the diagonal of the impression was seven times higher, that is 28 to 35 μm. The static parameters measured for enamel therefor cumulate the properties of the individual components and the structural features. The larger standard deviation of the results and thus the greater breadth of the measured values reflects the diversity of the substrate. On the length scale investigated in the present study, the observed viscoelastic behavior of the enamel can be seen as a consequence of frictional sliding[3] between hydroxyapatite crystallites, protein detachment from crystallites or deformation inside the crystallites.[38]

A similar approach has been considered for the measurements in dentin. In contrast to enamel, the parameters measured in dentin can be compared well with the data measured in RBCs. This is due to the lower hydroxyapatite content compared to enamel (70% by weight, 40–45% by volume).[39] The inorganic amount in dentin is accordingly in the range of the values given for the filler in RBCs in terms of the amount of filler by weight, but is much less in terms of the amount of filler by volume (Table 1). By this observation it can be inferred that dentin prevails a much higher density compared to the RBCs examined. This observation may explain the significantly higher E_{IT} and E' values measured in the dentin compared to the RBCs, with the exception of GSO, while the hardness of the dentin belongs to the lowest values measured. The microstructure of dentin is complex and must be seen as a puzzle of different types of dentin, reflecting different functions and bearing their own specificities.[39] In a general assessment, dentin is a porous, mineralized connective tissue with an organic matrix (collagenous proteins) and an inorganic component (hydroxyapatite). In contrast to measurements done in the enamel, the depth of indentation in dentin was higher and varied from 9 to 10 μm, while the diagonal of the impression were 63 to 70 μm. Similar to enamel, the measured properties therefore represent the properties of the substrate and not the properties of the individual substrate components.

Despite the fact that the damping behavior (tan δ) with the frequency differ among the analyzed RBCs and the tooth structures, a steady decrease in tan δ with the frequency prevailed in all analyzed substrates, while a plateau is reached only at high frequency (11.8 Hz). Regardless of their structural and compositional peculiarities and the associated different energy dissipation, all of the analyzed materials as well as the tooth structure are better adapted to the relevant frequency for chewing (0.94 to 2.17 Hz[8]) than for higher frequencies. This observation is consistent with the chemical composition of the RBCs analyzed, since the viscoelasticity of polymers is a result of polymer flexibility and the time it takes for a polymer chain to fully adapt to the applied stress.[7] The faster a stress is applied, the shorter the time available for the molecules to relax and accommodate that stress. In addition, the viscoelasticity observed in the analyzed RBCs has to be related to the structural features of the materials, since the main mechanism in stress dissipation is related to friction at the interphase boundary.[3] This can occur intra-molecularly, between the polymer chain and the filler, or between adjacent filler particles. In this context, the two ormocer-based RBCs showed the highest damping capacity, followed by BEG and BLS. The high damping capacity observed in the ormocer-based RBCs must be related to the friction occurring in the interface region between the nanoparticles and the matrix. Owing to the high inorganic filler amount (84 wt%, Table 1) and the small size of the particle, the effective interface region between polymer chains and nanofillers is large. In addition to friction, the lower crosslinks in the ormocer matrix[14] may act less restrictive to the thermal movements of molecular chains.[7] However, increase damping capacity in these materials lead to a decrease of strength and modulus of elasticity. On a different note, the high damping capacity observed at BEG and BLS must in addition be related to the prepolymerized fillers, which are only contained in these two materials. The amount of inorganic filler in these RBCs is therefore less than the specified total amount of filler (see Table 1 for BEG), which is clearly reflected in the lowest static parameters H_{IT} and E_{IT} as well as in the low strength and moduli of elasticity. It should be mentioned that both materials behave almost identically in terms of the measured properties. In contrast to the ormocers, all other RBCs contain a mixture of several methacrylates in their organic matrix with the inherent extreme and continuous structural heterogeneity and differing crosslinking density[40] which make an additional contribution to the dissipation of stress at these interphase boundaries.[3] On a general note, and taking into account the complex relationship between structure, composition and damping ability, a decreasing amount of inorganic phase (filler, Table 1) and an increasing amount of organic phase (polymer matrix) lead to an improved damping ability. At the same time, damping ability and static mechanical properties such as modulus of elasticity, strength, or indentation modulus proved to be mutually exclusive.

On a macroscopic scale, the reinforcing effect of fillers and their amount is best noticeable in the excellent strength and modulus of elasticity of GSO and the group of RBCs with nano- and agglomerated nanoparticles (FSE, FSB, and FSD). The scatter of the measured strengths was well modeled by Weibull statistics in all RBCs (Figure 1, Table 2). In this context, FSE, FSB, and especially FSD are characterized by the highest Weibull parameters and thus are the most reliable materials analyzed. This may be due to lower volume defects and better adaptability of the material to the walls of the matrix in the preparation of samples, since fracture originated in these RBCs very rarely from surface defects. Compared to GSO, this aspect is reflected in the highest FS values, while the lower amount of inorganic filler is evident in the lower modulus of elasticity and indentation modulus. The group of RBCs with nano- and agglomerated nanoparticles behave almost analogous with regard to their viscoelastic and quasistatic parameters and performed closest to dentin with regard to the storage modulus and damping capacity.

With the experimental data, all null hypotheses can be rejected. Large differences between RBCs and between RBCs and the tooth structure were found for all parameters measured and depending on the frequency.

5 | CONCLUSIONS

Many new dental RBCs configurations have emerged in recent years that deserve a thorough comparative investigation. Analyzed RBCs react to mechanical stress in close dependence on their microstructure and chemical composition. Their damping capacity has not yet been fully exploited, but it can be a parameter that should be correlated with clinical behavior. It can be modified by

acting on RBCs constituents, size, geometry and boundary conditions, and increased in the analyzed RBCs with decreasing amount of inorganic filler, while ormocers and RBCs with prepolymerized fillers exhibited the highest values. The damping capacity and the static mechanical properties such as modulus of elasticity, strength, and indentation modulus were mutually exclusive, which may reveal further strategies in the improvement of RBCs. Analyzed microhybrid RBCs are sufficient in relation to the dentin, but apart from the damping behavior, they perform inferior to the tooth enamel.

CONFLICTS OF INTEREST

The author declare no conflict of interest.

ACKNOWLEDGEMENT

The author is grateful to the manufacturer for supplying the analysed materials.

DATA AVAILABILITY STATEMENT

The datasets generated during and/or analysed during the current study are available from the corresponding author on reasonable request.

ORCID

Nicoleta Ilie https://orcid.org/0000-0002-6003-9199

REFERENCES

1. Ilie N. Spatial distribution of the micro-mechanical properties in high-translucent CAD/CAM resin-composite blocks. *Materials (Basel)*. 2020;13:1-16.
2. Ilie N, Hickel R, Watts DC. Spatial and cure-time distribution of dynamic-mechanical properties of a dimethacrylate nano-composite. *Dent Mater*. 2009;25:411-418.
3. Ti-S K. Experimental evidence of the viscous behavior of grain boundaries in metals. *Phys Rev*. 1947;71:533-546.
4. Chang H-H, Yeh C-L, Wang Y-L, et al. Differences in the biomechanical behaviors of natural teeth and dental implants. *Dent Mater*. 2021;37:682-689.
5. Yi Q, Feng X, Zhang C, et al. Comparison of dynamic mechanical properties of dentin between deciduous and permanent teeth. *Connect Tissue Res*. 2021;62:402-410.
6. Ilie N. Frequency-related viscoelastic properties in high translucent CAD-CAM resin-based composites. *J Mech Behav Biomed Mater*. 2021;118:104427.
7. Shaw T, MacKnight J. Introduction to polymer viscoelasticity. In: *Phenomenological Treatment of Viscoelasticity*, (ch. 2, pp. 7-50). WILEY Interscience; 2015.
8. Po JM, Kieser JA, Gallo LM, Tesenyi AJ, Herbison P, Farella M. Time-frequency analysis of chewing activity in the natural environment. *J Dent Res*. 2011;90:1206-1210.
9. Alvanforoush N, Palamara J, Wong RH, Burrow MF. Comparison between published clinical success of direct resin composite restorations in vital posterior teeth in 1995-2005 and 2006-2016 periods. *Aust Dent J*. 2017;62:132-145.
10. Ferracane JL. Resin-based composite performance: are there some things we can't predict? *Dent Mater*. 2013;29:51-58.
11. Heintze SD, Ilie N, Hickel R, Reis A, Loguercio A, Rousson V. Laboratory mechanical parameters of composite resins and their relation to fractures and wear in clinical trials-a systematic review. *Dent Mater*. 2017;33:e101-e114.
12. Fujimoto Y, Iwasa M, Murayama R, Miyazaki M, Nagafuji A, Nakatsuka T. Detection of ions released from S-PRG fillers and their modulation effect. *Dent Mater J*. 2010;29:392-397.
13. Ilie N, Hickel R. Investigations on mechanical behaviour of dental composites. *Clin Oral Investig*. 2009;13:427-438.
14. Bottenberg P, Alaerts M, Keulemans F. A prospective randomised clinical trial of one bis-GMA-based and two ormocer-based composite restorative systems in class II cavities: three-year results. *J Dent*. 2007;35:163-171.
15. Ferracane JL. Resin composite–state of the art. *Dent Mater*. 2011;27:29-38.
16. Ilie N, Fleming GJ. In vitro comparison of polymerisation kinetics and the micro-mechanical properties of low and high viscosity giomers and RBC materials. *J Dent*. 2015;43:814-822.
17. Roberts T, Miyai K, Ikemura K, Fuchigami K and Kitamura T, inventorsFluoride ion sustained release preformed glass ionomer filler and dental compositions containing the same 1999.
18. Ikemura K, Tay FR, Endo T, Pashley DH. A review of chemical-approach and ultramorphological studies on the development of fluoride-releasing dental adhesives comprising new pre-reacted glass ionomer (PRG) fillers. *Dent Mater J*. 2008;27:315-339.
19. Wolter H, Storch W, Ott H. New inorganic/organic copolymers (ORMOCERs) for dental application. *Mat res Soc Symp Proc*. 1994;346:143-149.
20. Moszner N, Gianasmidis A, Klapdohr S, Fischer UK, Rheinberger V. Sol-gel materials 2. Light-curing dental composites based on ormocers of cross-linking alkoxysilane methacrylates and further nano-components. *Dent Mater*. 2008;24:851-856.
21. Quinn GD. Room-temperature flexure fixture for advanced ceramics. NISTIR 4877. *National Institute of Standards and Technology*. 1992;1-26.
22. ISO 4049:2019 Dentistry. 2019 *Polymer-based restorative materials*. International Organization for Standardization:29.
23. ISO 14577-1:2015. 2015. *Metallic materials — instrumented indentation test for hardness and materials parameters — part 1: test method*. ISO:46.
24. Fischer-Cripps A. *Nanoindentation: Dynamic Indentation Testing*. Springer; 2004.
25. Weihull W. A statistical distribution function of wide applicability. *JApplMech*. 1951;18:290-293.
26. Pharr GM, Herbert EG, Gao Y. The indentation size effect: a critical examination of experimental observations and mechanistic interpretations. *Annu Rev Mat res*. 2010;40:271-292.
27. Cabibbo M, Ricci P. True hardness evaluation of bulk metallic materials in the presence of pile up: analytical and enhanced lobes method approaches. *Metallurgical and Materials Transactions A*. 2013;44:531-543.
28. Oliver WC, Pharr GM. Measurement of hardness and elastic modulus by instrumented indentation: advances in understanding and refinements to methodology. *Journal of Materials Research*. 2004;19:3-20.
29. McElhaney KW, Vlassak JJ, Nix WD. Determination of indenter tip geometry and indentation contact area for depth-sensing indentation experiments. *Journal of Materials Research*. 1998;13:1300-1306.
30. Herbert EG, Oliver WC, Pharr GM. Nanoindentation and the dynamic characterization of viscoelastic solids. *J Phys D Appl Phys*. 2008;41:074021.
31. Tweedie C, Van Vliet K. Contact creep compliance of viscoelastic materials via nanoindentation. *Journal of Materials Research - J MATER RES*. 2006;21:1576-1589.
32. Cheng L, Xia X, Scriven LE, Gerberich WW. Spherical-tip indentation of viscoelastic material. *Mech Mater*. 2005;37:213-226.
33. Wang L, Liu X. Characterization of viscoelastic materials by quasi-static and dynamic indentation. *Measurement Science and Technology*. 2014;25:064017.
34. Cheng L, Xia X, Yu W, Scriven LE, Gerberich WW. Flat punch indentation of viscoelastic material. *J Polym Sci B*. 2000;38:10-22.
35. Ramakers-van Dorp E, Haenel T, Sturm F, Möginger B, Hausnerova B. On merging DMA and microindentation to determine local mechanical properties of polymers. *Polymer Testing*. 2018;68:359-364.

36. Black J, Hastings G. Handbook of biomaterial properties. In: Dental Restoration Materials (Ch. 1d, pp. 191-203). London Chapman & Hall; 1998.
37. Maas MC, Dumont ER. Built to last: the structure, function, and evolution of primate dental enamel. *Evolutionary Anthropology: Issues, News, and Reviews*. 1999;8:133-152.
38. Ang SF, Bortel EL, Swain MV, Klocke A, Schneider GA. Size-dependent elastic/inelastic behavior of enamel over millimeter and nanometer length scales. *Biomaterials*. 2010;31:1955-1963.
39. Goldberg M, Kulkarni AB, Young M, Boskey A. Dentin: structure, composition and mineralization. *Front Biosci (Elite Ed)*. 2011;3:711-735.
40. Lovell LG, Berchtold KA, Elliott JE, Lu H, Bowman CN. Understanding the kinetics and network formation of dimethacrylate dental resins. *Polymers for Advanced Technologies*. 2001;12:335-345.

How to cite this article: Ilie N. Comparison of modern light-curing hybrid resin-based composites to the tooth structure: Static and dynamic mechanical parameters. *J Biomed Mater Res*. 2022;110(9):2121-2132. doi:10.1002/jbm.b.35066